P5.5

WSR-88D MANIFESTATIONS OF THE "OWL HORN" SIGNATURE

Matthew R. Kramar
National Weather Service WFO Amarillo, TX

1. INTRODUCTION

In prior conference forums, the "Owl Horn" Signature (OHS) was presented as identified from data obtained with the mobile X-band radar from the University of Massachusetts (Pazmany et al. 2003). Numerical simulations were conducted and also presented to determine the processes by which the signature forms. The signature was deemed to be of some operational utility, since, in all cases examined, storm splits occurred soon after the appearance of the OHS (helping to indicate the imminent severity of the storm). Also, in nearly every case (except for one storm, which was obliterated early in its life by a large linear complex of thunderstorms), the storms subsequently produced funnel clouds or tornadoes.

Since 2004, several instances of the OHS in WSR-88D data have been observed, some in very close proximity to the radar. All of these cases ultimately produced tornadoes.

This presentation will first review briefly the process by which the OHS is generated. It will then summarize meteorologically the most prominent WSR-88D cases since 2004 (including potential NWS operational impacts by considering the signature in warning decisions), and show where they fall in the spectrum of hodographs depicted in Kramar et al. (2005). Ultimately radar velocity data will be examined for consistency with the conceptual model of the OHS developed in Kramar et al. (2005).

Corresponding author address: Matthew R. Kramar, c/o WFO Amarillo, 1900 English Rd., Amarillo, TX 79108.
email: matthew.kramar@noaa.gov

2. REVIEW OF THE OHS CONCEPTUAL MODEL

By way of numerical simulations and TREC analysis (Kramar et al. 2005), it was determined that the OHS in reflectivity is a result of the presence of a pair of outflow thermal protrusions (outflow heads akin to those seen in Xu 1992) along the rear flanks of the exhibiting storm (Fig. 1a,b). In vertical cross-sections, the deeper head was found to have a vertical depth of at most 1.0 to 1.5 km and a horizontal scale of only 2.0 to 3.0 km each, and in general, it was noted that the left-flank outflow head was of much less vertical depth than its right flank counterpart. Narrow couplet bands of vertical vorticity were also diagnosed in the cross-sections, and were seen to flank the outflow protrusions. Trajectory analysis revealed that the OHS forms when the paths of small scatterers are influenced by the low-level vorticity couplets, and the scatterers are advected rearward into narrow appendages. It became clear, then, that the signature is a result of the development of these low-level vorticity couplets.

Further trajectory and vorticity analysis showed that the couplets themselves form as a result of the tilting of ambient parcels' streamwise horizontal vorticity (predominantly acquired via the significant

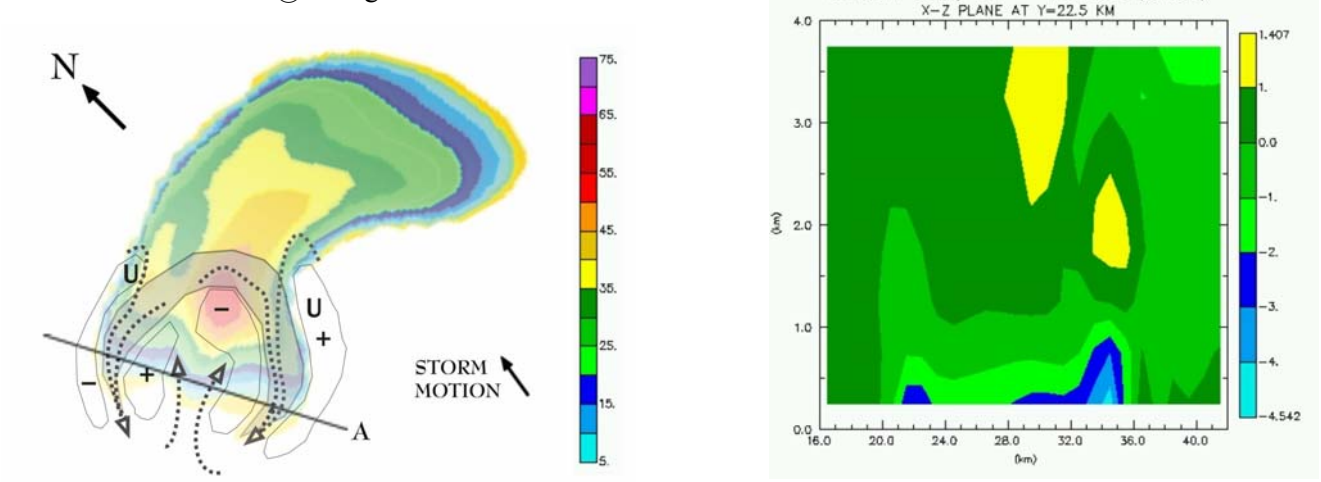

Fig. 1. (a) At left, a conceptual model of the OHS. U represents the storm updrafts, + and − represent cyclonic and anticyclonic vertical vorticity, stippled arrows represent sense of SRM flow, and shaded contour represents outflow protrusions. (b) At right, a cross section through the outflow protrusions along line A showing potential temperature perturbations in K.

low-level horizontal shear that often characterizes supercell near-storm environments, but also in very small quantity via baroclinic generation in close proximity to the outflow) as the parcels are lifted over the thermal protrusions in the expanding outflow (Fig. 2). The vorticity couplets in turn offer an enhanced wind channel through which the colder air in the thermal protrusions may be advected farther rearward, the protrusions amplified further, and the system momentarily circuitous before the outflow expands sufficiently to no longer influence scatterer trajectories.

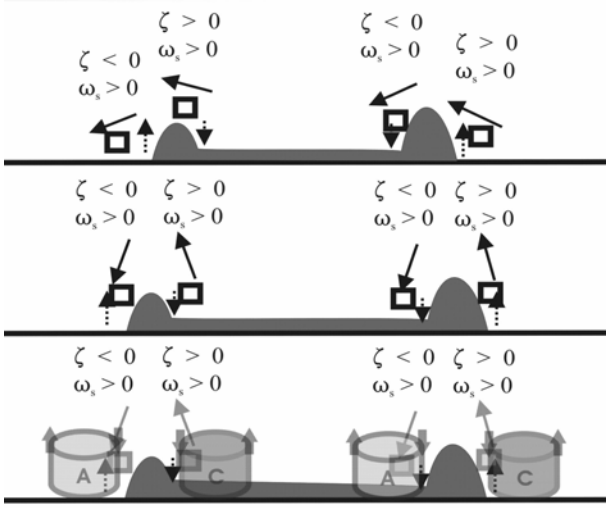

Fig. 2. Depiction in XZ plane of process by which vertical vorticity couplets are generated by outflow heads.

Kramar et al. (2005) concluded that the OHS was a precursor to storm splitting, supported by the nearly immediate storm splits that were observed subsequent to the appearance of the OHS, and by the appearance of midlevel features commonly associated with storm splits during or just prior to the formation of the OHS: a second midlevel cyclonic/anticyclonic vertical vorticity couplet resulting from a downward-directed midlevel pressure gradient (Bluestein and Sohl 1979; Klemp 1987; Bluestein 1993); and a second (younger and less vertically extensive) precipitation shaft along the left flank that eventually becomes the left-splitting cell (not shown).

A series of sensitivity test simulations was also conducted (after Adlerman and Droegemeier 2002), in which hodograph shape and magnitude were varied (with both supercellular and non-supercellular shear) to determine an effective spectrum of hodograph shapes and magnitudes within which an OHS might form. It was found that not only was supercellular shear (i.e. 0–6 km shear greater than 19 m s^{-1}) a requirement, but low-level curvature to the hodograph as well—that is, the straight-line hodograph that is known to produce symmetric splitting storms was shown to be incapable of producing an OHS. Table 1 (from Kramar et al. 2005) summarizes the hodographs used for the sensitivity tests.

3. WSR-88D CASES—ENVIRONMENTAL BACKGROUND

It was previously thought that the OHS would not be detectable by the WSR-88D owing to the radar's too-infrequent scanning pattern and too-coarse resolution, and so high-resolution data from the WSR-88D radar network was not initially examined for appearances of the signature. However, since 2004, several instances of the OHS in WSR-88D data have been observed, some in very close proximity to the radar. These cases include 5 May 2006 (near Seminole, TX), 17 June 2004 (near Borger, TX) and 21 June 2004 (northwest of Amarillo, TX). All of these cases ultimately produced tornadoes. We will examine herein the first and third of the cases.

a. 5 May 2006

The synoptic environment over West Texas was characterized by a somewhat moist and unstable airmass as depicted by the dry adiabatic lapse rates in the 6 May/0000 UTC MAF sounding and large area of higher dewpoints on the 6 May/0000 UTC surface map (Fig. 3). A frontal boundary was situated across the area, with a surface low inferred from the surface wind field over southeastern New Mexico. Moist air was observed behind the frontal wind shift as well. Aloft, a substantial trough was located near the Four Corners region.

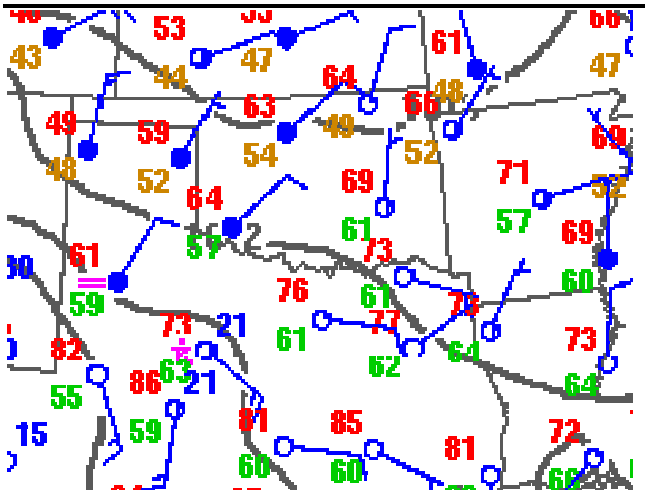

Fig. 3. Surface plot at 0000 UTC on 6 May 2006.

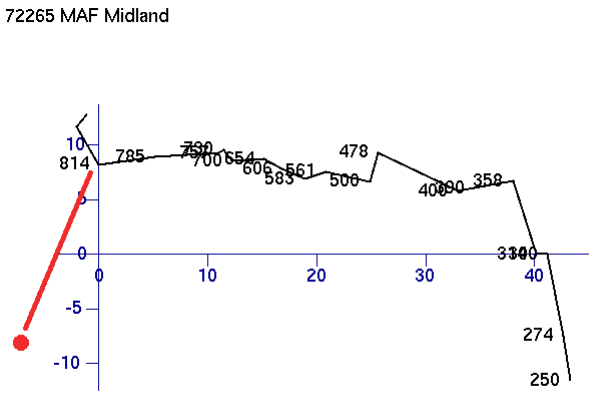

Fig. 4. Hodograph from 6 May/0000 UTC sounding released from MAF. Lowlevel modification in red assuming worst-case linear interpolation from surface wind field. Storm motion was to the southeast at 10 m s^{-1}.

An examination of the hodograph from the MAF sounding reveals what could be described as a near-straightline shape for much of the midlayers. Superficially, this wind environment would not be conducive to development of the OHS since significant low-level curvature is not present. However, the 5 May 2006 supercell near Seminole, TX was actually located just behind the windshift associated with the frontal boundary, in an area characterized by northeasterly winds of approximately 5 m s^{-1} (10 kt). Modifying the hodograph to reflect these lowlevel winds (Fig. 4), we note qualitatively a much more pronounced curvature in the lowlevels. With a storm motion toward the southeast, significant helicity can be realized in the lowlevels. Therefore, the near-storm environmental hodograph around Seminole, TX can be classified as exhibiting low-level curvature with a quasi-straightline profile above. By comparison to Kramar et al. (2005), this hodograph qualitatively resembles the quarter-circle hodograph (from 0 to 3 km) with a straightline tail above it (from 3 to 9 km).

b. 21 June 2004

Deep moisture had been present over the Texas Panhandle for several days, reinforced further by an overnight lowlevel jet. Throughout the day, a cold front was moving slowly south while a surface low pressure area developed over the southwestern Texas Panhandle. By late afternoon, a moist and very unstable airmass was in place, as noted in surface and upper air observations (not shown), lowlevel winds had become near easterly in response to the surface low, and a midlevel shortwave trough was approaching the Southern Plains.

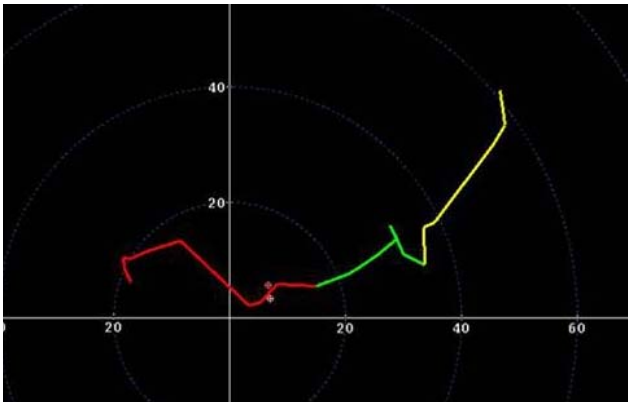

Fig. 5. Hodograph from 22 June/0000 UTC sounding released from AMA. Storm motion was to the southeast at 5 m s^{-1}.

The hodograph shape from the AMA sounding on 22 June 00 UTC (Fig. 5) is not quite as clear-cut as that from the MAF hodograph. Qualitatively, the hodograph depicts unidirectional flow in the midlevels and upper levels, with significant curvature in the lowlevels. This environment can be most closely compared to the quarter-circle hodograph with a straightline tail, but subject to a rotation of about 30°. The primary caveat is the weakness apparent in the wind field at about 750mb that alters the quarter circle shape somewhat.

4. 88D CASES—RADAR ANALYSIS

Ideal circumstances for radar sampling of the velocity field in an OHS would require that the primary axis of a storm be parallel to the radar beam, so that the vorticity couplets could be thoroughly diagnosed. The reality of these two cases is that the axes of the storms were more perpendicular to the radar beam, which at best allows us to diagnose convergence/divergence patterns of the couplets. In the conceptual model of the OHS (Fig. 1a), the right-flank outflow protrusion is bounded on the exterior by cyclonic vorticity and on the interior by anticyclonic vorticity. This structure would give rise to a convergence signature in storm-relative motion (SRM) slightly further downstream, with an area of weaker SRM flow along the cold air protrusion, where motion is more perpendicular to the radar beam. A nearly identical argument can be made along the left flank, which gives rise to a convergence-

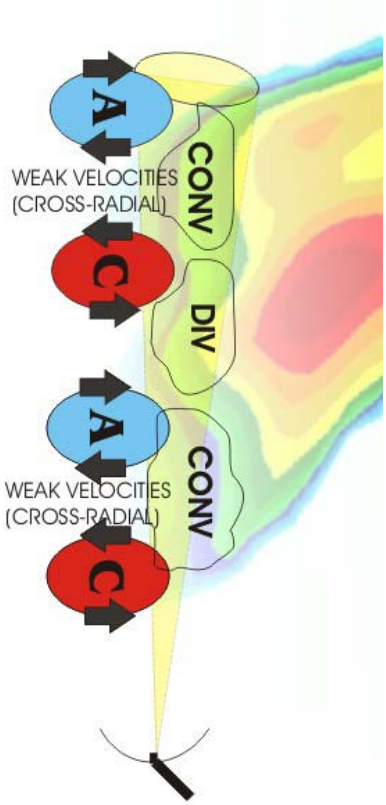

Fig. 6. Anticipated divergence and convergence signatures based on perpendicular sampling of an OHS by Doppler radar. The rotational aspect of the vertical vorticity would be muted, but a strong convergence signature would be expected along the right-flank appendage, with weaker convergence downstream of the left-flank appendage owing to the weaker strength of the left-flank couplet. Divergence would be expected between the two appendages.

divergence-convergence pattern associated with the OHS process under pure horizontal plane sampling (Fig. 6).

a. 5 May 2006

The OHS appeared most prominently between 2345 and 2359 UTC. The storm that exhibited the signature also contained a midlevel mesocyclone and had deviant motion toward the southeast, leading to its diagnosis as supercellular. The OHS is apparent at 2345 UTC (Fig. 7a) in the reflectivity pattern, and can be tracked as the storm evolves, with a second distinct maximum in reflectivity along the left flank becoming evident by 2354 UTC (Fig. 7c). This second maximum in reflectivity is a result of a left-splitting updraft that dissipates soon after separating from the parent updraft, a result consistent with Kramar et al. (2005).

At 2345 UTC (Fig. 7a), the SRM pattern began to exhibit signs of a weakness in the lowlevel flow as the OHS was forming in the reflectivity pattern, likely an indication of cross-radial storm-relative flow. By 2349 UTC (Fig. 7b), this pattern became much more prominent along both flanks, and the convergence-divergence-convergence structure diagnosed in Fig. 6 began to appear more clearly. The base velocity pattern in this time interval suggests even more clearly the structure of the outflow protrusions and convergence/divergence distribution.

Since the left-flank outflow protrusion is generally below 1 km in depth, and consequently would likely be missed in the non-horizontal PPI scans (especially at greater distances from the radar), and that in most circumstances the reflectivity signature would be observed. This instance of the OHS is remarkable in that the structure of both outflow protrusions appears to have been sampled quite well by the radar at an elevation of over 1200 m AGL and a distance of nearly 60 miles.

b. 21 June 2004

Because the 21 June OHS was much closer to the radar, the reflectivity signature presentation was much clearer by comparison, and several details of storm structure were also able to be diagnosed. The signature appeared most prominently between 2351 and 2359 UTC. The severity of the storm had already been determined by the presence of a large, rotating wall cloud, although radar indications also illustrated the supercellular nature of the storm.

A clear appearance of the impending OHS did not occur in reflectivity data until 2355 UTC. However, the right-flank gust front (fine line in reflectivity data) began to develop a kink along it by 2351 UTC (Fig. 8a), suggesting strong inflow into the updraft. Indeed, the curvature of the right-flank gust front is apparent, similar to gust front structure in simulated OHS storms. At 2355 UTC (Fig. 8b), the OHS reached its peak in reflectivity with a prominent left-flank appendage. As anticipated, this appendage evolved into a left-splitting storm by 2359 UTC (Fig. 8c).

The SRM pattern develops an apparent weakness between 2347 and 2351 UTC (just prior to the appearance of the OHS in reflectivity) (Fig. 8a), similar to that seen in the 5 May case. As a result, a diagnosis of a convergence-divergence pattern along the radial can be made. However, unlike the 5 May case, a complete convergence-divergence-convergence signature is not present in the SRM. This absence is likely a result of two conditions: although the storm was at a much closer position to the radar, the lowest PPI of the radar sampled the left-flank protrusion at just over 600 m AGL, which

simulations indicated is on the high end of depths for the left-flank protrusion; and the left-flank appendage has a component along the radial. The latter condition justifies the narrow zone of enhanced outbound velocities in both the SRM and base velocity products at 2355 UTC.

A noteworthy similarity is observed in both SRM products. The weakness in the SRM field (a result of cross-radial motion) behind the right-flank gust front is seen in base velocity products as an area of convergence beneath the updrafts of the storms. In both cases presented, it was along this area of convergence (and within 20 mins after the appearance of the OHS) that the first tornadic circulation developed. From a warning decision perspective, at the least, the OHS can alert the forecaster to the relative severity of the particular storm in comparison to other storms, and to its potential for focused lowlevel rotation. In the storms presented (as well as the storm on 17 June 2004), a tornado formed within 20 to 30 min after the appearance of the OHS, even absent a radar-detected tornadic vortex signature (TVS).

5. CONCLUSIONS

Two manifestations of the OHS on the WSR-88D were examined for consistency with the conceptual model presented in Kramar et al. (2005). While storm orientation precluded ideal analysis, it was shown that the convergence/divergence patterns in the velocity fields near the OHS are consistent with the conceptual model of the OHS. A common feature between the two cases was an area of cross-radial SRM flow (convergent flow) behind the right-flank gust front, that persisted after the dissipation of the OHS, and along which a subsequent tornado formed. While the dataset sample size is small, it is a striking curiosity (that bears further examination) that every storm that was observed with an OHS went on to produce a tornado or funnel cloud.

6. ACKNOWLEDGMENTS

Sincere thanks are extended to Brian Curran and Jeff Cupo at WFO Midland for providing radar data for the 5 May case; to Jamie Frederick at WFO Tulsa for providing radar data for a possible OHS case; to Jason Jordan at WFO Amarillo for collaborative analysis and to Rich Wynne for data assistance.

7. REFERENCES

Adlerman, E.J., and K.K. Droegemeier, 2002: The sensitivity of numerically-simulated cyclic mesocyclogenesis to variations in environmental parameters. *Preprints, 21st Conf. Severe Local Storms*, San Antonio, TX, Amer. Meteor. Soc., 264-267.

Bluestein, H.B., 1993: *Synoptic Dynamic Meteorology in Midlatitudes, Vol. II.* Oxford Univ. Press, 594pp.

_____, and C. Sohl, 1979: Some observations of a splitting severe thunderstorm. *Mon. Wea. Rev.* **107**, 861-873.

Klemp, J.B., 1987: Dynamics of tornadic thunderstorms. *Ann. Rev. Fluid Mech.*, **19**, 1-33.

Kramar, Matthew R., H.B. Bluestein, A.L. Pazmany and J.D. Tuttle, 2005: The "Owl Horn" radar signature in developing Southern Plains supercells. *Mon. Wea. Rev.* **133**, 2608-2634.

Pazmany, A.L., and F.J. Lopez, H.B. Bluestein, and M.R. Kramar, 2003: Quantitative rain measurements with a mobile, X-band, polarimetric Doppler radar. *Preprints, 31st Conf. Radar Meteorology*. Seattle, WA, Amer. Met. Soc., 858-859.

Xu, Q., 1992: Density currents in shear flows—A two-fluid model. *J. Atmos. Sci.,* **49**, 511-524.

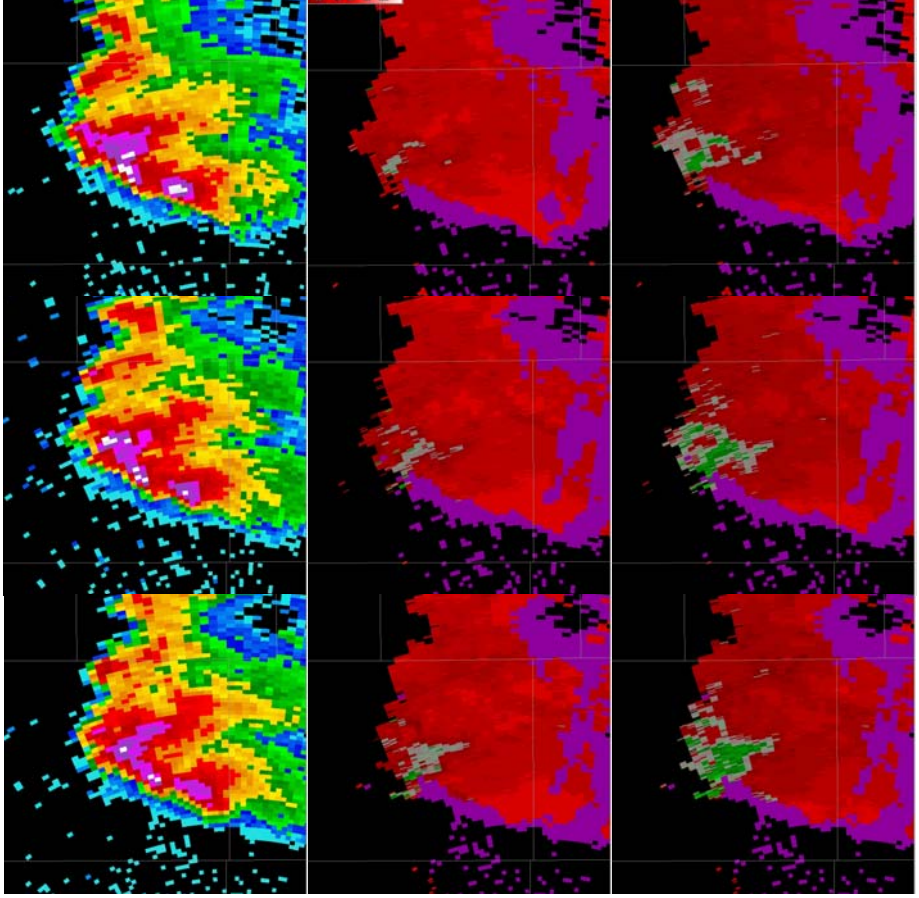

Fig. 7. (a) top, from left: 2345 UTC OHS from 5 May, reflectivity in dBZ; SRM in kt; base velocity in kt; (b) middle, same as in (a) but at 2349 UTC; (c) bottom, same as in (a) but at 2354 UTC.

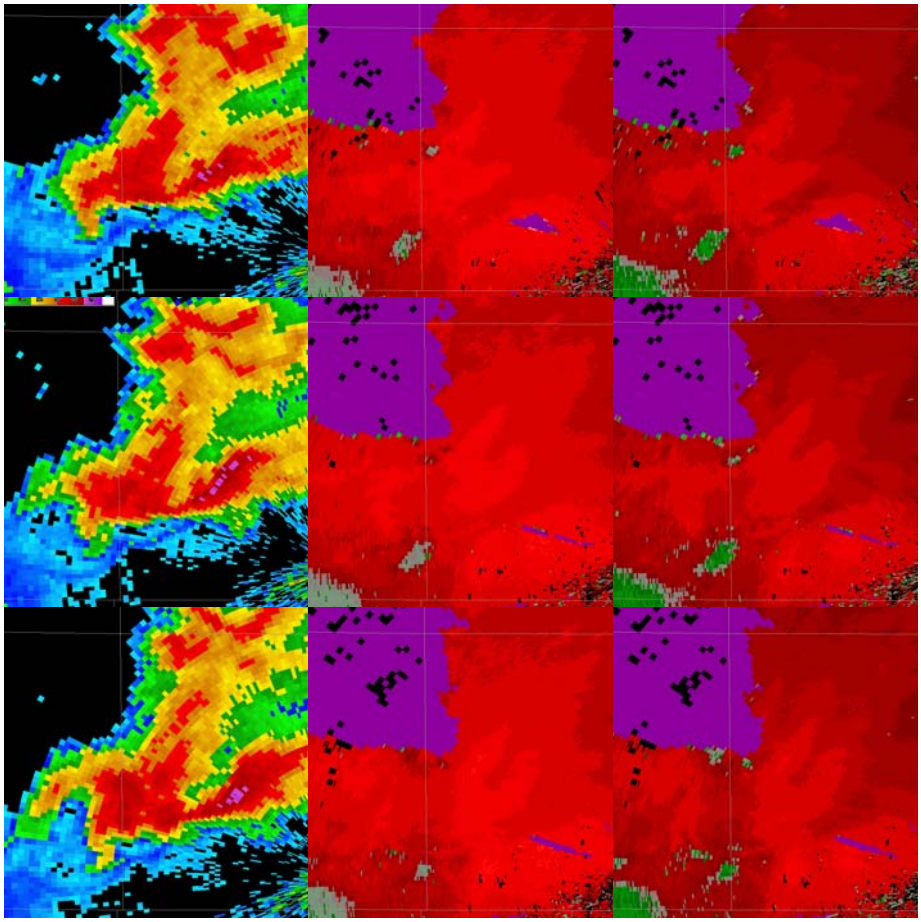

Fig. 8. (a) top, from left: 2351 UTC developing OHS from 21 June, reflectivity in dBZ; SRM in kt; base velocity in kt; (b) middle, mature OHS, as in (a) but at 2355 UTC; (c) bottom, same as in (a) but at 2359 UTC.